Dynamical coexistence of phases in molecular clusters

Ana Proykova and Stoyan Pisov
University of Sofia, Faculty of Physics, 5 James Bourchier Blvd., Sofia-1126, Bulgaria

R. Stephen Berry[a)]
The University of Chicago, Department of Chemistry, Chicago, Illinois 60637

(Received 27 November 2000; accepted 7 August 2001)

Two solid structures, a *bcc* orientationally disordered phase and a strained monoclinic orientationally ordered phase, may coexist for clusters of octahedral molecules. However, this coexistence is more difficult to observe in computer simulations of SF_6 clusters than of TeF_6 clusters although the SF_6 and TeF_6 molecules have the same symmetry. This study finds why this difference occurs. On the potential surface of the $(SF_6)_{89}$ cluster the relative energies of most of the linked minima differ only slightly, and the barriers between them are low. An exception is the global minimum, corresponding to a completely orientationally ordered phase. At relevant temperatures, the fraction of the available phase space of the $(SF_6)_{89}$ cluster corresponding to a partially ordered structure is smaller than it is for the $(TeF_6)_{89}$ cluster. In simulations, the latter readily exhibits coexistence of the ordered and disordered forms due to better separation of the higher-energy local minima and the larger available phase space volume. © *2001 American Institute of Physics.*
[DOI: 10.1063/1.1406976]

I. INTRODUCTION

Cluster phase transformations form a multifaceted field of study, involving the untangling of many-body physics spanning wide ranges of length- and time scales and describing thermal effects in phase spaces with complex topographies. Coexistence of two or more phaselike forms in finite systems occurs over *ranges* of temperatures, not just along curves, e.g., as given by $p_{\mathrm{vap}}(T)$, as it is in bulk.[1–3] In experiments, solid and liquid clusters coexist in an ensemble. Numerical simulations predict coexistence of solid and liquid regions in a single atomic cluster[4] and coexistence of two solidlike forms with different symmetries in a molecular cluster.[5]

Varieties of structures appears in molecular substances due to a space anisotropy of intermolecular potential. The transitions between the different structures involve both lattice reconstructions and orientation ordering, achieved by molecular rotation or its limited counterpart, libration. The vibration and rotation often couple to each other,[6] which makes impossible the decomposition of the molecular spectra into purely rotational and vibrational bands. The structural transitions could be discontinuous or continuous including cross-over between them. To distinguish between the two type of transitions is very difficult in the case of small systems. Recently, a classification scheme based on earlier works of Lee and Yang has been published.[7] Phase transitions are classified by analyzing the distribution of the zeroes of the canonical or grand canonical partion function in the complex temperature plane.

The coexistence of two structures is observable if a cluster spends time intervals long enough to establish characteristic equilibrium properties of each phase. A characteristic signature for coexisting phases is the bimodal form for the distribution of (short-term) mean kinetic and potential energy in microcanonical simulations or of the total and potential energy in the canonical simulations.[1,3]

Clusters of chalcogen hexafluorides, SF_6 and TeF_6, have been studied for more than two decades both experimentally[8,9] and theoretically[10–12] to understand their properties as functions of the temperature.

The simulated thermal behavior of SF_6 and TeF_6 clusters have been reported to be different,[13,14] namely that they exhibit different structures and different kinds of transitions on cooling or heating. The transitions in TeF_6 clusters have been recognized as continuous,[13] while those in SF_6—as discontinuous.[14] It is intriguing that coexisting phases have not been observed in the latter case. This result arises the question if the transition has been correctly ascribed.

It seems very instructive to investigate the origin of the differences in thermal behavior of free SF_6 and TeF_6 clusters and to establish the nature of their structural phase changes. This knowledge will be useful in controlling the transitions among the varieties of cluster forms, which may have both fundamental and technological importance.

In this research we show that a rich variety of complex phenomena in condensed matter arises from well-understood, simple underlying interactions among constituents. The parametrization of the interaction potential, which matches specific substance properties, can change the minima-to-saddle ratios without shifting the location of these extrema in the phase space but nevertheless changing the system's dynamics.

The paper is organized as follows: Section II presents the model for computer simulations of the thermal behavior of clusters made of 59 and 89 SF_6 and again 59 and 89 TeF_6 molecules; Sec. III gives the results that are the basis for our

a)Electronic mail: berry@uchicago.edu

conclusions in Sec. IV (with only the results for the larger clusters presented here). In the Appendix we analyze the perturbative effect of the time–space discretization on the trajectories of classical Hamiltonian systems.

II. MICROCANONICAL CALCULATION OF THERMAL EVOLUTION OF CLUSTERS

We have simulated the thermal behavior of clusters consisting of 59 and 89 rigid molecules of SF_6 or TeF_6, presenting only the results for the latter here. The clusters are initially arranged in the orientationally disordered *bcc* structure observed just below the clusters' freezing points. Details of the spatial arrangement are given elsewhere.[12,15]

The classical equations of motion of an N-molecule system with $n=6(N-1)$ degrees of freedom (the center of masses is fixed and the system as a whole is not allowed to translate)

$$\frac{d\mathbf{p_i}}{dt} = -\frac{\partial}{\partial \mathbf{q_i}} H(\mathbf{p_1}, \mathbf{q_1}, \ldots, \mathbf{p_N}, \mathbf{q_N}), \tag{1}$$

$$\frac{d\mathbf{q_i}}{dt} = \frac{\partial}{\partial \mathbf{p_i}} H(\mathbf{p_1}, \mathbf{q_1}, \ldots, \mathbf{p_N}, \mathbf{q_N}), \tag{2}$$

where $\mathbf{p_i}$ and $\mathbf{q_i}$ are the momenta and the positions of the ith particle, determine the trajectory $[\mathbf{p}(t), \mathbf{q}(t)]$, that the system follows in its $2n$-dimensional phase space. For systems in which the Hamiltonian has no explicit time dependence, $H = H(\mathbf{p}, \mathbf{q})$ and the energy E_{tot} of the system is conserved.

The integration of Eqs.(1) and (2) for $n \gg 1$ is performed by replacing the differential equations (1) and (2) with finite-difference equations. The step Δt of time discretization influences both the energy conservation of a Hamiltonian system and the stability of the trajectory in the phase space $(\mathbf{p}, \mathbf{q})$.

Equations (1) and (2) have been integrated at a constant total energy using the velocity Verlet algorithm[16,17] with a specially controlled time step (see Sec. III), which makes it possible to maintain the constancy of the energy at a high level of accuracy (10^{-5}), even in the vicinity of the phase transitions. The difficulty in this region is that of the huge fluctuations of the quantities involved. The truncation errors imposed on the fluctuating values play a perturbative role (Appendix) and may destabilize the trajectory of the system.

Previously, most of the simulations based on the velocity Verlet algorithm have been performed with an integration step of 10 fs.[12–15]. This step is good enough to maintain the energy constant for relatively short runs of about 10 000 integration steps. Because we need long runs to observe dynamical coexistence,[4,5] we have tested the ability of this algorithm to maintain the total energy as a function of the time step Δt of integration. For a 10 fs time step, the energy is conserved at 10^{-4} for about 0.5 ns. For longer runs the accuracy rapidly decreases. A very small Δt would maintain the energy much better, but the computation time would become unrealistically long and, worse still, the truncation errors start to play important role. Hence, the choice of Δt should simultaneously satisfy two requirements: To be much shorter than the characteristic time τ and to be large enough to make the computations efficient in the sense we discuss in the Appendix. (A much stricter test would be the duration of the period in which mechanical reversibility is maintained; we have found in previously unpublished tests that the first breakdown of precise mechanical reversibility may appear after only about 5000 time steps. Moreover doubling the precision of the calculation only doubles the length of this interval, which implies that the computer roundoff error introduces a chaotic character in the results.)

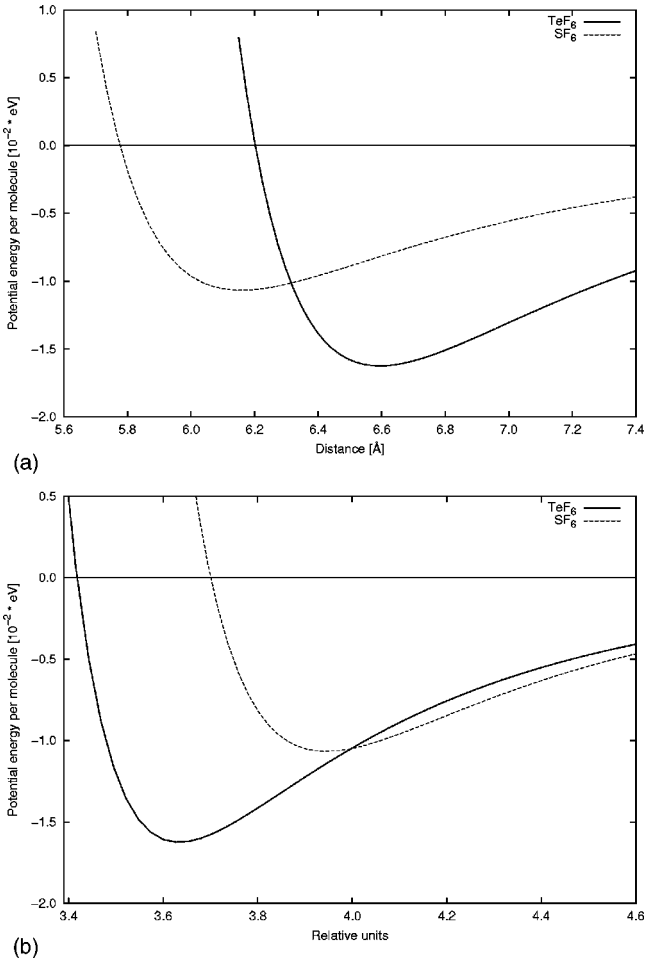

FIG. 1. Pairwise potentials for TeF_6 and SF_6 molecules.

Our previous molecular dynamics simulations of the thermal behavior of TeF_6 clusters showed that detecting phase coexistence is a very challenging task[5] for molecular systems. These simulations require long runs (about 1 ns and about 5 ns for clusters of 89 and 137 molecules, respectively); they require slow temperature changes $\triangle T \in (0.1-1)$ K in the vicinity of phase changes, more like annealing than quenching; and they require a careful choice of the integration step, in order to meet the two opposing requirements of being small enough to preserve the total energy (for constant-energy simulations) and large enough to allow computation of a long trajectory within a reasonable time.

Within the Born–Oppenheimer approximation,[17,18] it is possible to express the classical Hamiltonian $H(p,q)$ of the system as a function of the nuclear coordinates and momenta, with the rapid motion of the electrons averaged out.

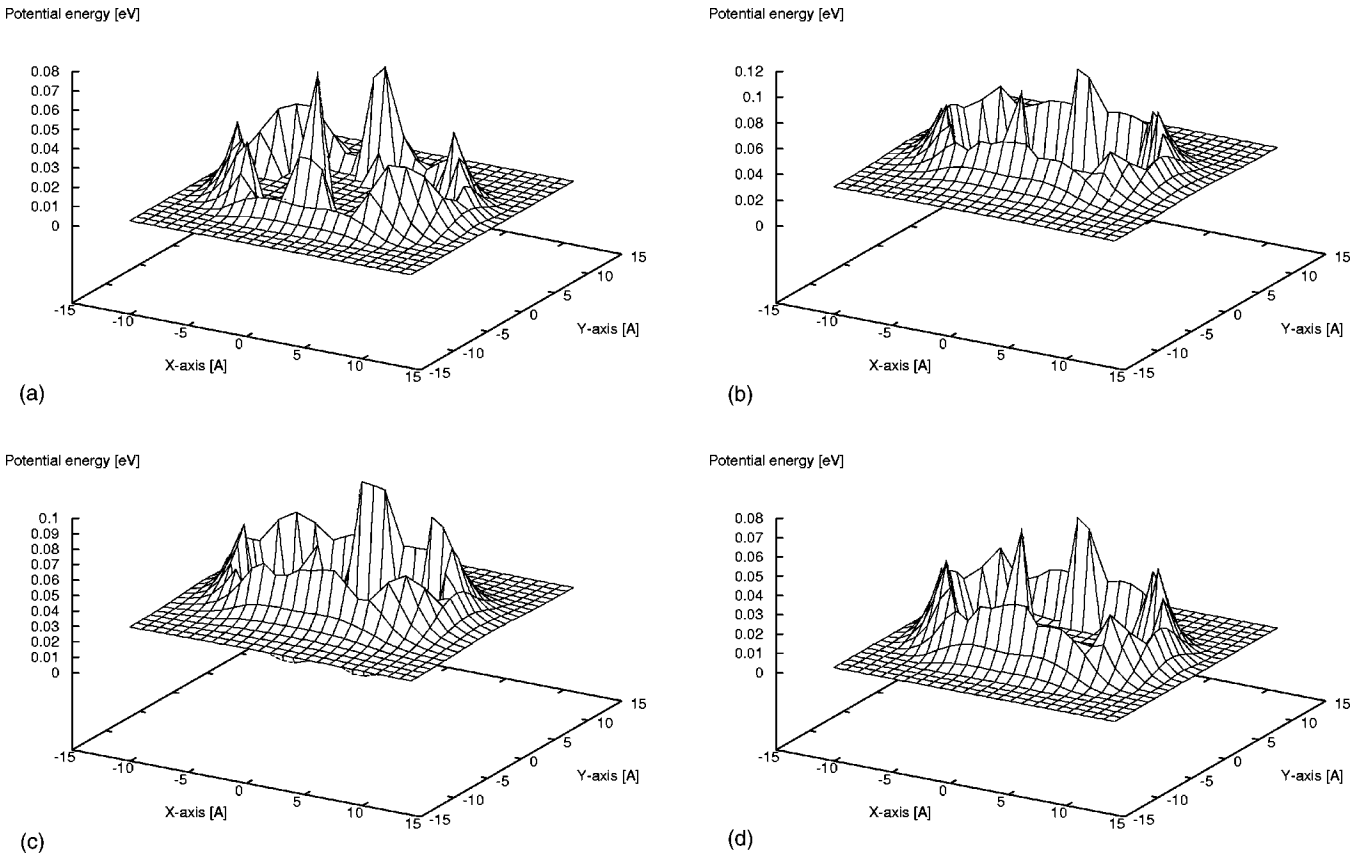

FIG. 2. Potential surface of a configuration of three molecules: Two molecules are fixed at a distance of 6.18 Å, and the third molecule probes the potential field. The orientations (in Euler angles in degrees) are as follows: (a) first molecule(0,0,0), second molecule(0,0,0) third molecule(0,0,0); (b) first molecule(0,45,0), second molecule(0,45,0), third molecule(0,0,0); (c) first molecule(0,45,0), second molecule(0,45,0), third molecule(0,45,0); (d) first molecule(0,0,0), second molecule(0,0,0), third molecule(0,45,0).

Then we write: $H=K+E_{\text{pot}}$, with K being the kinetic energy $K=\Sigma_{i=1}^{n}0.5(m\mathbf{v}_i^2+I\omega_i^2)$, where I is the tensor of inertia of each molecule with a linear $\mathbf{v}$ and angular ψ velocity. For octahedra, I is diagonal in a system fixed at the molecular center of masses. The anisotropy of the interaction potential has been accounted for by a double summation over pairwise atom–atom interactions[12,13]

$$U_{pw}(i,j)=\sum_{\alpha,\beta=1}^{7}\left[4\,\epsilon_{\alpha\beta}\left[\left(\frac{\sigma_{\alpha\beta}}{r_{ij}^{\alpha\beta}}\right)^{12}-\left(\frac{\sigma_{\alpha\beta}}{r_{ij}^{\alpha\beta}}\right)^{6}\right]+\frac{q_{i\alpha}q_{j\beta}}{4\pi\epsilon_0 r_{ij}^{\alpha\beta}}\right], \tag{3}$$

$$U_{pot}=\sum_{i,j=1\,(i<j)}U_{pw}(i,j), \tag{4}$$

where r_{ij} is the distance between the ith and the jth atom. The indices α and β denote either a fluorine or a tellurium (sulphur) atom. The following values for $\sigma_{\alpha\beta}$ in Å and $\epsilon_{\alpha\beta}$ in eV reproduce the experimental diffraction patterns:[13]

For TeF_6, $b=1.815$, $\sigma_{\text{Te,Te}}=4.294$, $\sigma_{\text{Te,F}}=3.553$, $\sigma_{\text{F,F}}=2.940$, $\epsilon_{\text{T,T}}=0.01376$, $\epsilon_{\text{T,F}}=0.00531$, $\epsilon_{\text{F,F}}=0.002\,049$;

for SF_6, $b=1.561$, $\sigma_{\text{S,S}}=3.405$, $\sigma_{\text{S,F}}=3.165$, $\sigma_{\text{F,F}}=2.943$, $\epsilon_{\text{S,S}}=0.012\,60$, $\epsilon_{\text{S,F}}=0.002\,72$, $\epsilon_{\text{F,F}}=0.002\,18$.

The Coulomb interaction accounts for[10,12] the effective electro-negativity of the fluorine atoms, $q_{\text{F}}=-0.1e$.

The interaction potential of two equivalent molecules, TeF_6 or SF_6, is plotted in Fig. 1 for the case of molecular symmetry axes aligned in space. In Fig. 1(a) the distance is in angstrom units and the interaction between two SF_6 molecules minimizes at a smaller distance In order to eliminate the difference in molecular sizes we should rescale the distance with the bond length b of the molecules, $b=1.561$ Å for SF_6 and $b=1.815$ Å for TeF_6. The potential re-plotted in this relative unit shows that (effectively) the SF_6 molecules are more separated in the cluster. One result is an easier reorientation of the SF_6 molecules. As a consequence, the depths of most wells of the multidimensional potential energy surface (PES) of SF_6 clusters are smaller than those of TeF_6 clusters, with the exception of the global minimum for SF_6, which is very steep, narrow, and deep. Because of that, it occupies only a tiny portion of the phase space available to the system with a moderate amount of energy or a moderately high temperature, so, under those conditions, the probabilistic measure of the global-minimum configuration is very small and the system rarely finds it.

III. RESULTS

In the current study, the numbers of molecules of SF_6 and TeF_6 in a free cluster are kept the same in order to check

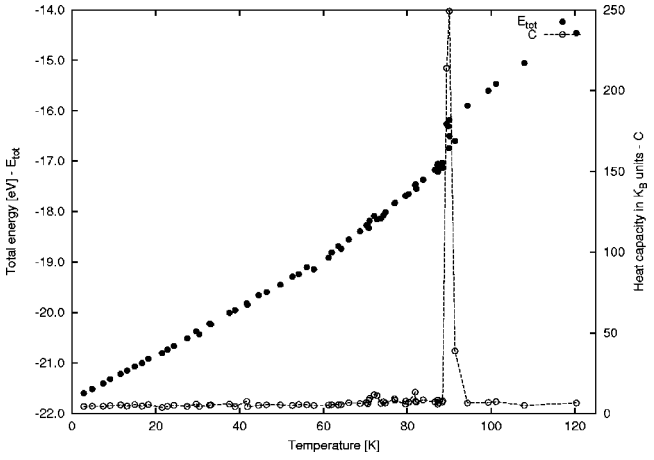

FIG. 3. Caloric curve and the heat capacity for a $(TeF_6)_{89}$ cluster. The heat capacity is computed from the energy fluctuations and is plotted in k_B units.

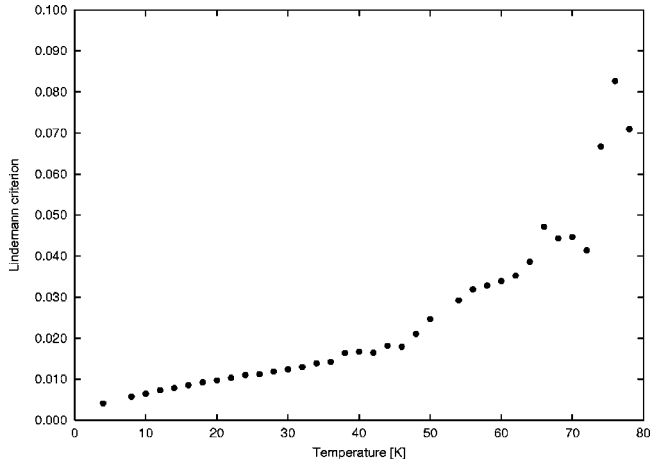

FIG. 5. Lindemann index for $(SF_6)_{89}$ clusters: Solid–solid transformations are observed at $\approx$40 K and $\approx$60 K. The jump at $\approx$80 K shows the solid–liquid transition.

if the potential parameters and molecular sizes and mass, rather than their symmetry, are responsible for the differences in the kinds of transitions one observes. If symmetries differ, one generally expects that the Hamiltonian space symmetry plays a large role in determining the system's properties. However, in the clusters of interest, the symmetries are the same, and we must look to finer characteristics to understand their differences. For these octahedral molecules, the interaction potential Eq. (4) is defined in a multiparametric manifold. The behavior of such complex systems may change with the values of the parameters.[19] This makes intuitive predictions based only on space-symmetry analysis rather uncertain as was demonstrated with Fig. 1.

Figure 2(a)–2(d) is a plot of the potential energy surface (minima are reversed, so the local wells point upward in the plot) in the simplest case of a three-body system: Two molecules, specifically oriented in the space, generate a potential that is seen by a third molecule at a given orientation. The relative spatial orientation of the molecules is described by the Euler angles θ, ϕ, ψ. To produce the figure we select an (x,y) plane, which contains the centers of the three molecules and fix the z-coordinate. The first two molecules are kept at a distance 6.18 Å along the x axes. Hence the x,y coordinates of these molecules are $(-3.09,0)$ and $(+3.09,0)$, respectively. The third molecule scans the x,y-plane from $(-\infty,-\infty)$ to $(+\infty,+\infty)$ with a small step.

The relative depths of the PES minima change for different mutual orientations of the three molecules, as this figure shows. The potential energy is in eV and the minima are deeper for cases (a) and (c), corresponding to aligned molecules. In case (a), the symmetry axes of the three molecules are parallel to each other. In case (c), each molecule is rotated at 45° in the respective plane following the Euler representation.[17]

The clusters explore their configuration space by crossing energy barriers that divide the PES into wells where locally stable structures (isomers) are formed. The ability of a system with total energy $E_{\rm tot}(T)$ to escape from a given well and to reach a transition state is given with its rate constant determined by the microcanonical version[4] of Rice–Ramsperger–Kasel–Marcus (RRKM) theory[20] as:

$$K_{\rm rate} = \frac{g}{h\,\rho(E^*)} \sum_{E^\dagger=0}^{E_{\rm tot}-E_{\rm ts}} \rho(E^\dagger),$$

where $\rho(E^*)$ is the density of states at $E^* = E_{\rm tot} - E_{\rm min}$, $E_{\rm min}$ is the local minimum, $\rho(E^\dagger)$ is the density of states at $E^\dagger = E_{\rm tot} - E_{\rm ts}$, $E_{\rm ts}$ is the energy of the transition state or saddle. The constant g accounts for possible existence of equivalent re-organizations of the cluster that are physically distinct in terms of labeled molecular geometry. The transition state could be in the rigid region for a given cluster size or in its nonrigid region. The density of states of the nonrigid limiting case increases rapidly with energy, faster than that of the rigid limit case. This increase is even faster if the level spacings of the nonrigid case are smaller than the vibrational separations of the rigid limit.

The potential energy surface has been mapped using the technique reported in Ref. 21. The relative number of saddle points is almost twice as great for an $(SF_6)_{89}$ cluster as it is for a $(TeF_6)_{89}$ cluster. We compute from the PES

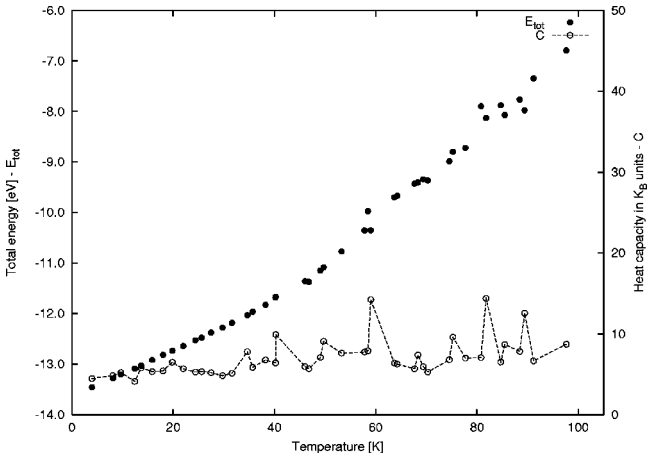

FIG. 4. Caloric curve and the heat capacity for a SF_6 cluster. The heat capacity is computed from the energy fluctuations and is plotted in k_B units.

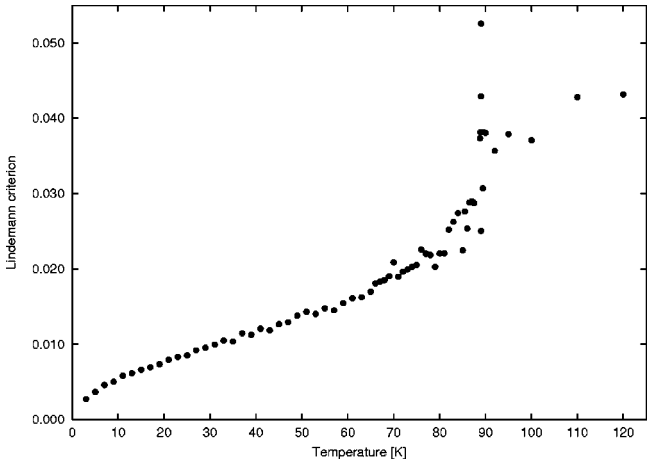

FIG. 6. Lindemann index for $(TeF_6)_{89}$ clusters: The slope of the curve changes in the region of 60 K indicating a continuous transition. The jump at ≈ 90 K shows lattice reconstruction but the cluster is solid.

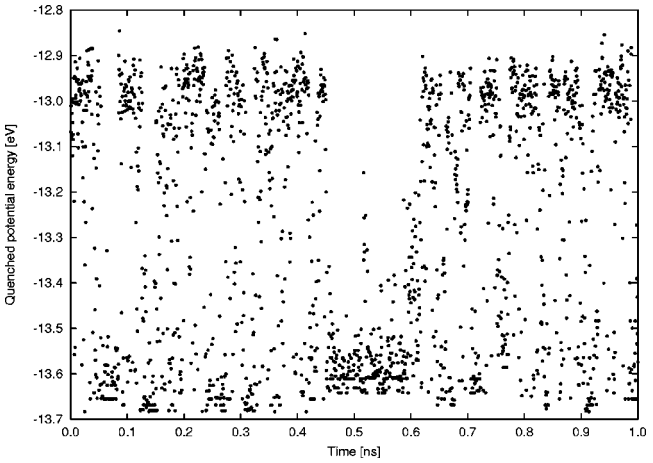

FIG. 8. Coexistence of two solid structures in a $(SF_6)_{89}$ cluster at $T=58.5$ K can be easily detected in the quenched structures. These phases can be distinguished in an IR (infrared) experiment.

$$(K_{\text{rate}})_{SF_6}/(K_{\text{rate}})_{TeF_6}=1.87.$$

Hence the SF_6 cluster spends less time than the tellurium cluster in any specific well. Because of that, the observation of coexisting phases is more difficult with SF_6 than it is with TeF_6.

In order to detect coexisting phases, we should know the characteristic vibrational period $\tau=\omega^{-1}$. This quantity can be estimated from the Einstein harmonic approximation, which gives an upper limit for τ

$$\omega=\sqrt{\frac{k_{ii}}{m}}, \tag{5}$$

where k_{ii} are the diagonal elements of the Hessian matrix $Hess=\partial^2/\partial\mathbf{r}\partial\mathbf{r}\,U(\mathbf{r})$. An analytic treatment of $Hess$ is not possible for a multiparametric potential U. To compute ω we have numerically determined the second derivative of U for a configuration of two molecules with their symmetry axes aligned. Replacing the curvature values in Eq. (5), in the case of the (0, 0, 0) orientation of the molecules, we determine

for two TeF_6 molecules $\omega\approx 408$ GHz, $\tau\approx 2.45$ ps,

for two SF_6 molecules $\omega\approx 442$ GHz, $\tau\approx 2.26$ ps. If one molecule is oriented at (0, 0, 0) and the other is at (45, 0, 0), then

for two TeF_6 molecules $\tau\approx 2.57$ ps,

for two SF_6 molecules, $\tau\approx 2.38$ ps.

These characteristic times are all of the same order of magnitude and show that the mutual orientation, (0, 0, 0) and (45, 0, 0), corresponds to a little more stable state than the former, (0, 0, 0) and (0, 0, 0).

The frequency computation lets us use one and the same integration step for both sulphur and tellurium clusters, e.g., $\Delta t=5$ fs, which is approximately 1/500 of τ.

To detect dynamical coexistence of two or more phases,[4] the cluster should be in equilibrium. This means that the thermalization time at a prescribed temperature should be at least one order of magnitude greater than the characteristic vibrational period. Runs of 50–100 ps have been performed to thermalize the system by rescaling the vibration and rotation velocities of each molecule[12] until $\langle E_{\text{kin}}\rangle_{\text{vib}}=\langle E_{\text{kin}}\rangle_{\text{rot}}$. Much longer runs, 1–5 ns, were then carried out at a constant

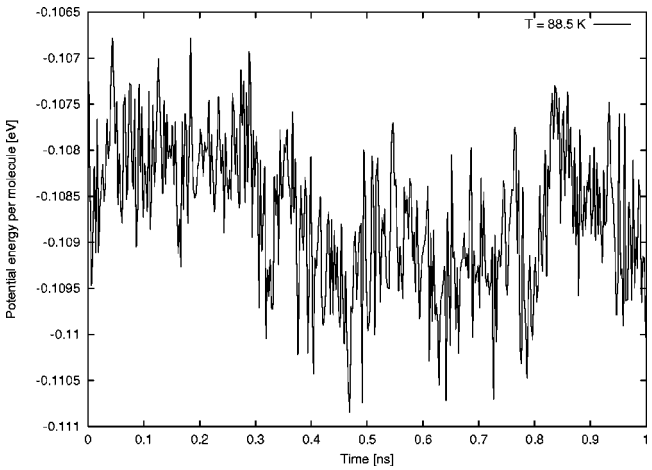

FIG. 7. Coexistence of a liquidlike and solidlike phases in an $(SF_6)_{89}$ cluster at $T=88.5$ K.

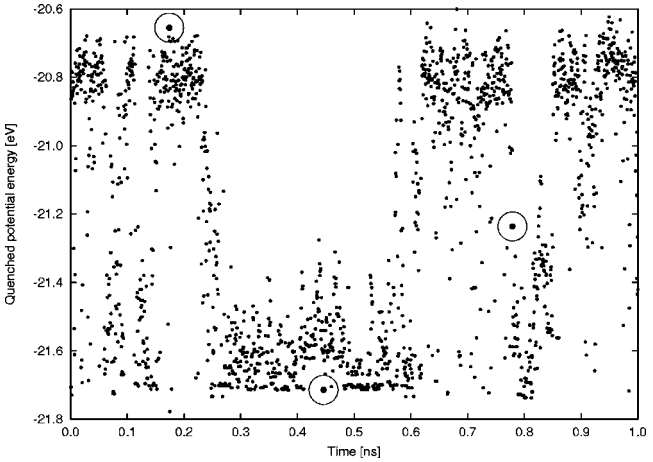

FIG. 9. Coexistence of two solid structures in a $(TeF_6)_{89}$ cluster at $T=89.4$ K. The transition temperature is higher for a cluster consisting of larger-size molecules.

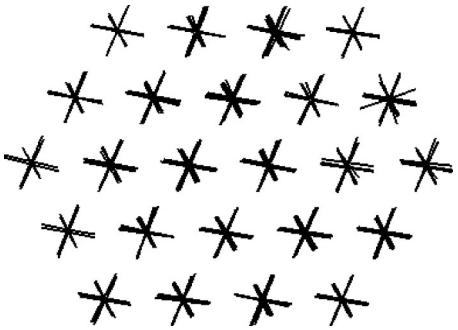

FIG. 10. Frame 21: A view from the partially orientation ordered monoclinic structure. There is no orientation order in the plane perpendicular to the one shown, (x,y).

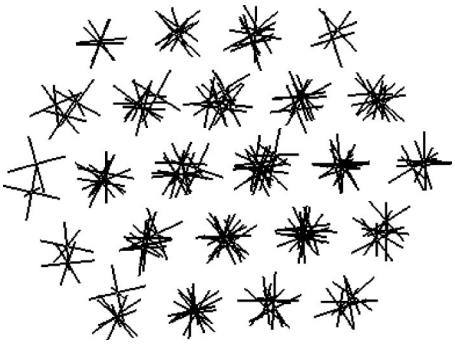

FIG. 12. Frame 60: Orientationally disordered cubic structure.

energy to obtain the evolution of the potential energy. After a run is completed the effective, mean temperature T is computed from the mean kinetic energy

$$\langle E_{\mathrm{kin}}\rangle = \frac{3(N-1)k_B T}{2},$$

where the bracket denotes averaging either the *vibration* kinetic energy or the *rotation* kinetic energy over the run time (without the thermalization time) and k_B is the Boltzmann constant. The difference between the pre-selected temperature and the computed one is larger (up to 15%) in the vicinity of phase changes.

Another important condition for detecting coexisting phases is a sufficiently slow temperature rate of cooling–heating.[5] A rugged potential energy surface requires a change of the system's temperature slow enough to avoid trapping in a metastable state. If this trapping happens, the system cannot escape from a local minimum for realistic computational times. The local minimum acts as if it were an attractor inducing a quasi-periodic orbit. In such a situation, the phase space available to the system is not properly spanned.

The caloric curves and the heat capacity for $(TeF_6)_{89}$ and $(SF_6)_{89}$ clusters are given in Figs. 3 and 4, respectively. The caloric curves are derived directly from the simulations and the mean kinetic energy. The heat capacities have been computed from the fluctuations of the potential energy in a microcanonical ensemble. We have modified the Lebowitz formula[22] to make it applicable in the vicinity of phase transitions as follows:

$$C/k_B = \frac{3}{2}\left[1 - \frac{3}{2}\frac{(N-1)^2}{N}\frac{\langle \delta T^2\rangle}{\langle T\rangle^2}\right]^{-1}.$$

The comparison of the two figures clearly shows the different behavior of the $(TeF_6)_{89}$ and $(SF_6)_{89}$ clusters. The tellurium cluster has a well-resolved jump in the heat capacity at the upper-temperature solid–solid transition, while the values of the heat capacity in the $(SF_6)_{89}$ clusters are of the same order of magnitude for the three transitions in the temperature region (0–90 K): At about 80 K is a liquid–solid transition as the Lindemann criterion shows, Fig. 5; at about 60 K there is a solid–solid transition, disordered cubic-to-monoclinic, a discontinuous transition; and at about 40 K, there is another solid–solid transition, disordered-to-ordered monoclinic.

To distinguish between the liquid–solid and solid–solid transitions, we have computed the Lindemann index, δ_{lin}, from

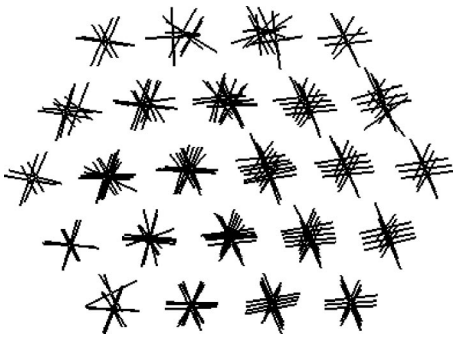

FIG. 11. Frame 33: Dynamical coexistence of two solid structures: in several hundreds of pico-seconds the cluster transforms either to a structure seen in Frame 21, or transforms back to a disordered cubic structure, Frame 60.

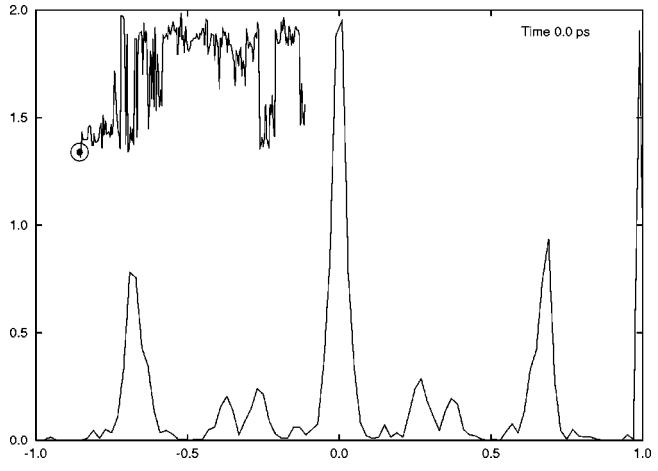

FIG. 13. The distribution of the molecular axes of symmetry averaged over all molecules. The peaks at 0 and 1 correspond to indistinguishable mutual orientations: aligned $[\cos 0=1]$ and perpendicular $[\cos \pi/2=0]$, because rotation of $\pi/2$ does not change the octahedral molecule. The inset shows the change of the potential energy as a function of the molecular orientations and the time in ps. The lowest lying state indicated with a circle corresponds to a complete orientation order: All the molecular axes of symmetry are aligned as in the Fig. 10.

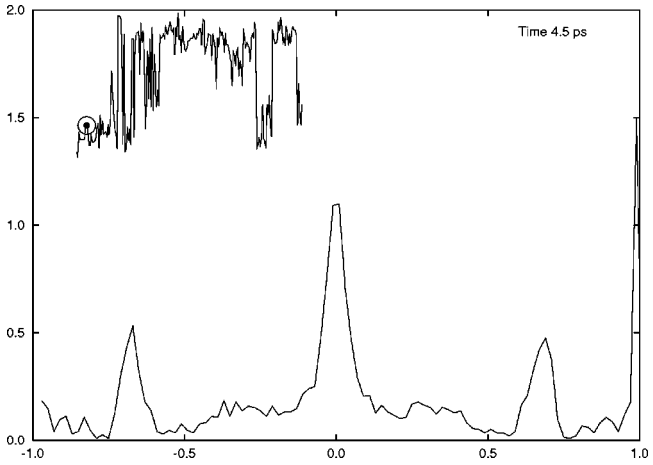

FIG. 14. The decrease in potential energy for less ordered molecules.

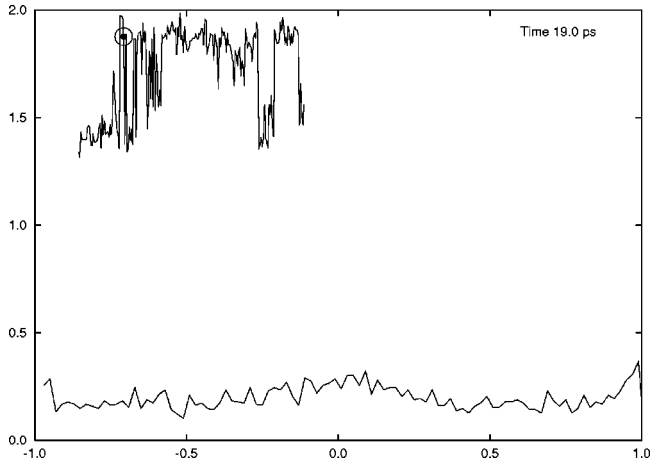

FIG. 16. The uniform population of orientations at the highest potential energy.

$$\delta_{\mathrm{lin}}=\frac{2}{N(N-1)}\sum_{i,j(>i)=1}^{N}\frac{\sqrt{\langle r_{ij}^2\rangle-\langle r_{ij}\rangle^2}}{\langle r_{ij}\rangle}, \tag{6}$$

where $|i\mathbf{r}_{ij}|=|\mathbf{r}_i(t)|-|\mathbf{r}_j(t)|$ and $\langle . \rangle$ denotes time averaging. For bulk, $\delta_{\mathrm{lin}}\geqslant 0.1$ corresponds to a melted phase. In free clusters, due to the surface, δ_{lin} is size-dependent and is less than 0.1 for a fluid phase. More precise estimation of the melting temperature can be obtained from the slope of δ_{lin} for a given cluster size, i.e., from $\partial\delta_{\mathrm{lin}}/\partial T$.

The plot in Fig. 5 shows that the sulphur cluster is completely melted at $T=80$ K while the tellurium cluster with the same number of molecules is solid, Fig. 6. The shift of the transition temperatures towards lower values for the case of the SF_6 cluster can be estimated from Fig. 4. The lower melting temperature is consistent with the softer potential in Fig. 1(b). Let us remember that changing the range and curvature at the minimum of the pair potential has a strong effect on the shape of the multidimensional surface, which in turn determines the dynamics of the system.[23]

The simultaneous analysis of Figs. 3–6 shows that the two solid–solid transformations ($\delta\ll 0.1$) occur at ≈ 90 K and ≈ 60 K for a $(TeF_6)_{89}$ cluster and at ≈ 60 K and ≈ 40 K for an $(SF_6)_{89}$ cluster. In both cases the transition temperatures rescale from the sulphur cluster to its tellurium counterpart with a factor ≈ 1.5.

The liquid–solid transformation of the $(SF_6)_{89}$ cluster at ≈ 80 K is discontinuous and we observe a clear picture of coexisting phases, Fig. 7. The upper-temperature solid–solid transformation (60 K for SF_6 and 90 K for TeF_6) is also discontinuous, the finite-system analogue of a first-order transition as well, and we consequently observe a temperature band of phase coexistence in the simulations, Figs. 8 and 9. This phase change is associated with a reconstruction of the lattice, as easily seen from the slope of $\delta_{\mathrm{lin}}(T)$ in the region above 90 K and below 85 K for $(TeF_6)_{89}$, Fig. 6. Due to the smoother topography of its potential, the SF_6 cluster spends less time in each minimum associated with one of the phases. The second solid–solid transformation (60 K for TeF_6 and 40 K for SF_6) is continuous and is related to a spatial ordering of the molecular orientations. There is no reorganization of the lattice as the smooth variation in the Lindemann index shows. In this region there is no phase

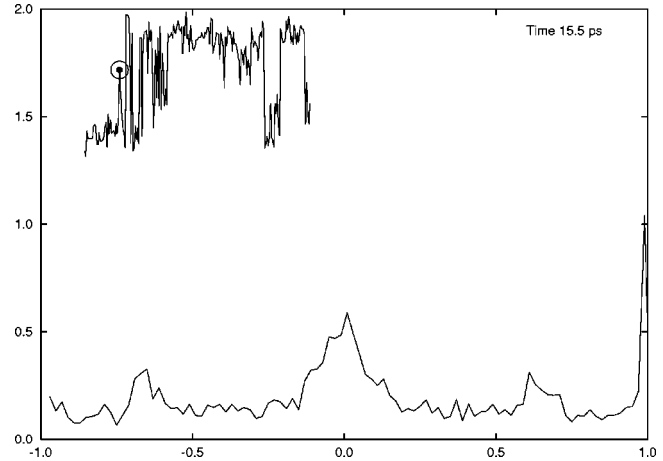

FIG. 15. Partial order of the molecular axes of symmetry—the potential energy is high.

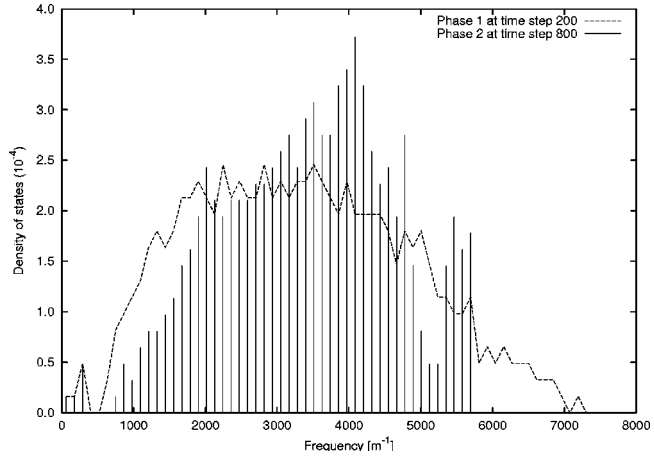

FIG. 17. Density of the vibration states, multiplied by a factor of 10^4, of the two quenched structures of an 89-molecule TeF_6 cluster at ≈ 90 K. The long tail of the density distribution at the time step 200 indicates disorder of the lattice.

coexistence, so that this phase change fits the traditional theory of critical phenomena for second-order transitions, with a single minimum in the free energy.

In order to detect coexisting solid structures, we have quenched the molecular dynamics (MD) trajectory in the upper temperature transition region, at ≈ 90 K for $(TeF_6)_{89}$ and at ≈ 60 K for $(SF_6)_{89}$. Quenching is a means to associate arbitrary points in the phase space with the local minima in whose wells they lie on the PES.[24] We have used the conjugate gradient method[25] to minimize the energy of the MD trajectory. At the end of every 250 fs interval, we have recorded the quenched structures and have subsequently performed normal mode analysis.

The plot of the quenched potential energy Fig. 8 indicates two well-resolved states in the sulfur cluster after quenching: One state, A_1, has a total binding energy of approximately -12.95 eV and the other, state A_2, lies at approximately -13.61 eV. The equilibrium constant for the transition between the phase A_1 and the phase A_2 is estimated from: $K=$(amount of time spent in A_1)/(amount of time spent in A_2)$=1.58$, which indicates that the state with the ordered molecular axes is less favorable for this system, at $T=58.5$ K, the transition temperature of this simulation.

The quenched potential energy of a tellurium cluster in the transition region is plotted in Fig. 9, for $T=89.4$ K. The system spends almost the same amount of time in the two solid phases: Cubic (with orientational disorder) and monoclinic (with partial order). The evolution of the cluster, seen in animations,[26] shows that the orientational ordering transformations are initiated at the surface.

The diagrams of Figs. 10–12 show three snapshots from an animation (indicated with circles in Fig. 9): Frames 21, 33, 60, taken at times 200, 450, and 780 ps, respectively. Frame 21 shows a quenched structure ordered along the *z* axis, but is orientationally disordered in the *xy*-plane, while Frame 60 shows a cubic, orientation-disordered structure. Frame 33 clearly demonstrates two coexisting structures. At temperatures below the second, lower solid–solid transition, all axes become orientation ordered.

A better monitoring of the order gives the distribution of the mutual orientation of the molecules. This distribution is a function of the temperature, of course, and changes during the run, due to the dynamics. Figures 13–16 show the evolution of the orientation distribution in the transition region, where the systems transform from one structure to another.

Finally, the vibrational spectrum, shown in Fig. 17, indicates that the system adopts two slightly different lattices along its MD trajectory, namely in the intervals around time steps 200 and 800.

Due to the small lattice reconstruction, the cluster can transform between the two structures in an observable period of time. We must point out that a very small change of the temperature, about 0.1 K, is enough to bring the cluster into the upper- or the lower-energy phase for time intervals longer than the duration of a reasonable computation, 6–10 ns. Only by careful tuning of the temperature was it possible to detect the coexistence of these two phases, and, thereby, to demonstrate the existence of two local minima in the free energy for this phase change.

IV. CONCLUSION

The thermal behavior of TeF_6 and SF_6 clusters consisting of the same number of octahedral molecules have been studied both analytically and numerically to find the reason for an apparent discrepancy in their phase behavior published in the literature. We show that the general properties of the transitions observed in the two systems are very similar, i.e., both systems transform from a highly symmetrical state, a *bcc* structure with complete disorder of the molecular orientation axes of symmetry, to a lower-symmetry lattice, first with partially ordered (aligned), and then, at lower temperatures or energies, with completely ordered molecular axes. For the finite-system analogue of a first-order transformation, we observe phase coexistence by inspecting the time evolution of the potential energy.

A detailed analysis of the topography of PES reveals the reason for the phases of the SF_6 clusters being more difficult to distinguish than those of the TeF_6 cluster: The smoother landscape of the sulfur PES increases the rate constants for transitions between neighboring minima. This decreases the time the system spends in any specific phase. Because of that, one must perform very long runs, with a carefully selected step of integration Δt and with enough slightly different initial points in the phase space in order to avoid quasiperiodic orbits generated by truncation of the numbers in the computers.

ACKNOWLEDGMENTS

NATO Grant CLG SA(PST.CLG.976363)5437 is acknowledged. This work has been funded by a Grant from National Science Foundation. Two of the authors (A.P. and S.P.) acknowledge partial support from the University of Sofia Scientific Fund, Grant No. 3270/1999-2000.

APPENDIX: PERTURBATION OF INTEGRABLE HAMILTONIAN SYSTEMS

The complicated energy surface of a molecular cluster imposes specific requirements for performing reliable calculations. On one hand, Liouville's theorem states that the phase space volume for Hamiltonian systems is incompressible. As a consequence, Hamiltonian systems do not have attractors in the usual sense of having bounded subsets to which regions of initial conditions of nonzero phase space volume converge asymptotically with increasing time.

We consider systems in which the Hamiltonian has no explicit time dependence, $H=H(\mathbf{p},\mathbf{q})$ and the energy E_{tot} of the system is conserved. A basic structural property of Hamiltonian's equations is that they are *symplectic*. That is, if we consider three orbits that are infinitesimally displaced from each other, $(\mathbf{p}(t),\mathbf{q}(t))$, $(\mathbf{p}(t)+\delta\mathbf{p}(t),\mathbf{q}(t)+\delta\mathbf{q}(t))$ and $(\mathbf{p}(t)+\delta\mathbf{p}'(t),\mathbf{q}(t)+\delta\mathbf{q}'(t))$, where $\delta\mathbf{p}$, $\delta\mathbf{q}$, $\delta\mathbf{p}'$, and $\delta\mathbf{q}'$ are infinitesimal *n* vectors, then the quantity

$$\delta\mathbf{p}\cdot\delta\mathbf{q}'-\delta\mathbf{q}\cdot\delta\mathbf{p}',$$

which is called the differential symplectic area, is independent of time

$$\frac{d}{dt}(\delta\mathbf{p}\cdot\delta\mathbf{q}'-\delta\mathbf{q}\cdot\delta\mathbf{p}')=0.$$

The symplectic condition is the same as Liouville's theorem for $n=1$, while for $n>1$ the symplectic condition is more fundamental.[19] We are interested in $n\gg1$ which means that we study the symplectic condition for preservation of phase space volume.

The calculation of Eqs. (1) and (2) for $n\gg1$ is performed by replacing the differential equations (1) and (2) with finite-difference equations. The step Δt of time discretization influences both the energy conservation of a Hamiltonian system and the trajectory's $(\mathbf{p},\mathbf{q})$ stability.

We study temperature-driven phase transitions of a Hamiltonian system and particularly, dynamical coexistence of phaselike forms. In order to observe such phenomena, we should follow the trajectory $(\mathbf{p},\mathbf{q})$ for a time t long enough for the system to exhibit oscillations and diffusion characteristic of a specific phase, so that we should choose $t\sim100\Sigma_i\tau_i$, where τ_i is a characteristic vibrational period of the ith phase. Here we meet the competing sources of errors: Δt and the truncation error limited by the number of digits carried by our digital computer. If we decrease Δt, then the computational time increases and inaccuracy due to the accumulated error increases. The choice of Δt can be optimized of course but at any instant, the truncation acts as a small perturbation γ, which effectively changes the Hamiltonian $H'(\mathbf{p},\mathbf{q})$

$$H'(\mathbf{p},\mathbf{q})=H(\mathbf{p},\mathbf{q})+\gamma H_1(\mathbf{p},\mathbf{q}).$$

Then we should expect that for a typical form of perturbation, $H_1(\mathbf{p},\mathbf{q})$, all the constants of motion for the integrable system, $H'(\mathbf{p},\mathbf{q})$, except the constant energy, $E=H'(\mathbf{p},\mathbf{q})$, are immediately spoiled as soon as $\gamma\neq0$. For small γ, orbits would initially approximate the orbits of an integrable system, staying close to unperturbed n-tori that exist for $\gamma=0$ for at least short times.

The initial Hamiltonian $H(\mathbf{p},\mathbf{q})$ is integrable and satisfies the requirement of having n-independent constants of motion f_i. The last implies that the trajectory of the system in phase space is restricted to lie on an n-dimensional surface: $f_i(\mathbf{p},\mathbf{q})=k_i;\ i=1,\ldots,n$, where the k_i are constants.

For constants of motion f_i, the Poisson bracket is $\{f_i,H\}=0$, and it is known that $\{f_i,f_j\}=0$ for each $i,j=1,\ldots,n$. This restricts the topology of the surface, $f_i(\mathbf{p},\mathbf{q})=k_i$, to be of certain type: It must be an n-dimensional torus. Thus for integrable systems, the phase space is completely occupied by n-tori, almost all of which are filled by n-frequency quasiperiodic orbits. In contrast to the case of n-frequency quasiperiodicity is the case of true periodic motion, in which orbits on the n-torus close on themselves. Thus, arbitrarily near any torus on which there is n-frequency quasiperiodicity, there are tori on which the orbits are periodic. On a complex PES, the trajectories wander and a small random perturbation, caused for example by truncation error, might lead the system to one or another set of tori, possibly far distant from the first.

What do we gain from this analysis? First, it gives us a way to relate the results of different computations to the lengths of the computational times and the truncation errors that induce a perturbation H_1 in the initial Hamiltonian. This in turn might bring the system to a temporary periodic orbit. In such a case the system spends some time in a restricted region of the phase space, which acts temporarily as if it were an attractor. Excepting the total energy, the studied quantities have different values when averaged over a trajectory with or without ''attractors.''

Second, the analysis explains why, in some simulations, people do not detect phase coexistence: to observe this, the trajectory must visit the phases several times during the run and should stay in each long enough (at least tens of vibrational periods) in order to obtain a proper averaging of the fluctuating quantities, the kinetic and the potential energy.

[1] R. S. Berry, in Phase Transitions **24–26**, 269 (1990).
[2] D. J. Wales, J. Chem. Phys. **91**, 7002 (1989).
[3] R. S. Berry, in *Theory of Atomic and Molecular Clusters*, edited by J. Jellinek (Springer-Verlag, Berlin, 1999) pp. 1–26.
[4] R. E. Kunz and R. S. Berry, Phys. Rev. E **49**, 1895 (1994).
[5] A. Proykova, S. Pisov, R. Radev, I. Daykov and R. S. Berry, in *Proc. of the Second Workshop on Nanoscience*, edited by E. Balabanova (Heron Press, Sofia, 2001).
[6] A. Proykova, D. Nikolova, and R. S. Berry, http://xxx.lanl.gov/abs/physics/9911049
[7] P. Borrmann, O. Mülken, and J. Harting, Phys. Rev. Lett. **84**, 3511 (2000).
[8] L. S. Bartell, L. Harsami, and E. J. Valente, NATO ASI Ser., Ser. B **158**, 37 (1987).
[9] J. Farges, M. F. de Feraudy, B. Raoult, and J. Torchet, J. Chem. Phys. **78**, 5067 (1987).
[10] F.-Yi Li, R. S. Berry, and A. Proykova, in *Book of Abstracts of Middle-West Theoretical Conference on Chemistry, May 12–16*, Evanston, IL, 1995.
[11] K. E. Kinney, Shimin Xu, and L. S. Bartell, J. Phys. Chem. **100**, 6935 (1996).
[12] A. Proykova and R. S. Berry, Z. Phys. D: At., Mol. Clusters **40**, 215 (1997).
[13] L. S. Bartell and Shimin Xu, J. Phys. Chem. **95**, 8939 (1991).
[14] J. B Maillet, A. Boutin, S. Buttefey, F. Calvo, and A. H. Fuchs, J. Chem. Phys. **109**, 329 (1998).
[15] A. Proykova, R. Radev, Feng-Yin Li, and R. S. Berry, J. Chem. Phys. **110**, 3887 (1999).
[16] L. Verlet, Phys. Rev. **159**, 98 (1967).
[17] M. P. Allen and D. J. Tildesley, *Computer Simulation of Liquids* (Clarendon, Oxford, 1994).
[18] S. E. Koonin, *Computational Physics* (Addison-Wesley, New York, 1986).
[19] E. Ott, *Chaos in Dynamical Systems* (Cambridge University Press, Cambridge, 1993).
[20] P. J. Robinson and K. A. Holbrook *Unimolecular Reactions* (Wiley-Interscience, London, 1972).
[21] K. Ball, R. S. Berry, R. Kunz, F.-Y Li, A. Proykova, and D. Wales, Science **271**, 963 (1996).
[22] J. B. Lebowitz, J. K. Percus, and L. Verlet, Phys. Rev. **153**, 250 (1967).
[23] J. P. Rose and R. S. Berry, J. Chem. Phys. **96**(1), 517 (1992).
[24] F. H. Stillinger and T. A. Weber, Kinam **3**, 159 (1981).
[25] W. H. Press, S. A. Teukolsky, W. T. Vetterling, and B. P. Flannery, *Numerical Recipes* (Cambridge University, Cambridge, 1986).
[26] S. Pisov, A. Proykova, and R. S. Berry, to appear in the electronic journal Int. J. Mol. Sci. ISSN 1422-0067 http://www.mdpi.org/ijms/